LAWRENCE
LIVERMORE
NATIONAL
LABORATORY

LLNL-JRNL-416290

A new urban boundary layer and dispersion parameterization for an emergency response modeling system: tests with the Joint Urban 2003 data set

Luca Delle Monache, Jeffrey Weil, Matthew Simpson, Marty Leach

August 28, 2009

Atmospheric Environment

Disclaimer

A new urban boundary layer and dispersion parameterization for an emergency response modeling system: tests with the Joint Urban 2003 data set

Luca Delle Monache[a,b], Jeffrey Weil[c], Matthew Simpson[a], Marty Leach[a]

[a]*Lawrence Livermore National Laboratory, Livermore, California, USA*

[b]*Now at National Center for Atmospheric Research, Boulder, Colorado, USA*

[c]*Cooperative Institute for Research in Environmental Sciences, University of Colorado, Boulder, Colorado, USA*

Revised Manuscript submitted to Atmospheric Environment, 25 July 2009

Corresponding author:

Luca Delle Monache, Research Applications Laboratory, National Center for Atmospheric Research, PO Box 3000, Boulder, CO 80307-3000, USA. Phone: +1 303 497 2736. Fax: +1 303 497 8386. E-mail address: lucadm@ucar.edu.

Abstract

A new urban parameterization for a fast-running dispersion prediction modeling system suitable for emergency response situations is introduced. The parameterization represents the urban convective boundary layer in the dispersion prediction system developed by the National Atmospheric Release Advisory Center (NARAC) at Lawrence Livermore National Laboratory. The performance of the modeling system is tested with data collected during the field campaign Joint Urban 2003 (JU03), held in July 2003 in Oklahoma City, Oklahoma. Tests were performed using data from three intense operating periods held during daytime slightly unstable to unstable conditions. The system was run in operational mode using the meteorological data that would be available operationally at NARAC to test its effectiveness in emergency response conditions. The new parameterization considerably improves the performance of the original modeling system, by producing a better degree of pattern of correspondence between predictions and observations (as measured by Taylor diagrams), considerably reducing bias, and better capturing directional effects resulting in plume predictions whose shape and size better resemble the observations (via the measure of effectiveness). Furthermore, the new parameterization shows similar skills to urban modeling systems of similar or greater complexity. The parameterization performs the best at the three JU03 sensor arcs (1, 2, and 4 km downwind the release points), with fractional bias values ranging from 0.13 to 0.4, correlation values from 0.45 to 0.71, and centered root-mean-square error being reduced more than 50% in most cases. The urban parameterization has been tested with grid increments of 125, 250, 500 and 1000 m, performing best at 250

and 500 m. Finally, it has been found that representing the point source by a Gaussian distribution with an initial spread of particles leads to a better representation of the initial spread induced by near-source buildings, resulting in lower bias and improved correlation downtown Oklahoma City.

Keywords: urban parameterization, dispersion modeling, emergency response.

1. Introduction

The adaption of efficient strategies to protect public health from an accidental or deliberate release of a hazardous contaminant into the atmosphere in urban environments is key to successful emergency response operations. Such strategies require an understanding of dispersion processes which can be facilitated by accurate and timely predictions. It is challenging to produce such predictions because the often complex atmospheric flow in the boundary layer can be substantially modified by the presence of a city (Bornstein, 1975; Oke, 1988; Arya, 2001). One of the more accurate modeling approaches may involve building-aware computational fluid dynamics (CFD) methods coupled with dispersion models to predict the temporal and spatial evolution of the atmospheric contaminant (e.g., [Chan and Leach, 2004] and [Chan and Leach, 2007]; Flaherty et al., 2007b). However, CFDs are computationally very expensive, and cannot be used currently for emergency response purposes, when the predictions may be needed by decision makers on the ground in a matter of minutes.

Recently there have been several contributions towards urban parameterizations for atmospheric dispersion modeling (e.g., Brown, 2004; Piringer and Joffre, 2005; Hendricks et al., 2007; Warner et al., 2008; Hanna and Baja, 2009; Hanna et al., 2009). In this paper, a new urban parameterization to represent the urban convective boundary layer for a mass-consistent fast-running dispersion modeling system is presented (Section 3). This system is designed to satisfy emergency response requirements, where an accurate prediction needs to be produced in a timely manner—in a few minutes. The urban parameterization has been designed to be implemented in a prediction system that

includes the Atmospheric Data Assimilation and Parameterization Techniques (ADAPT) model and the Lagrangian Operational Dispersion Integrator (LODI) model. ADAPT and LODI were developed by the National Atmospheric Release Advisory Center (NARAC) at Lawrence Livermore National Laboratory (LLNL) for operational emergency response dispersion predictions (Nasstrom et al., 2007). The ADAPT/LODI modeling system is not building-aware, and therefore is expected to produce in a few minutes concentration estimates averaged over spatial scales of a minimum of few hundreds of meters. In Section 5.2.1 the performance of the new approach is explored with different grid increments.

The new urban dispersion prediction capability is tested with one of the most comprehensive field campaigns in urban environments, the Joint Urban 2003 (JU03) that was conducted in July 2003 in Oklahoma City, Oklahoma (Allwine et al., 2004). The goal of JU03 was to collect meteorological and tracer data at several different scales, going from the individual city block, to the flow in the central business district (CBD), up to scales of a few kilometers downwind of the CBD of Oklahoma City.

To test the prediction system effectiveness in emergency response conditions, the simulations have been performed with the same meteorological data that would be available for NARAC operations, i.e., five surface stations distributed around the city (from 10 to 60 km from the release locations) and upwind upper air data available at the Norman airport about 25 km South of the CBD. The existing modeling system is introduced in the following section, and the details of the new urban parameterization are given in Section 3. The JU03 and the simulations set-up are described in Section 4. Results are presented in Section 5, followed by conclusions and a summary in Section 6.

2. Modeling system description

In this section a general description of the modeling system employed in this study is given. Specific aspects that have been modified in the models to account for the effect of urban roughness elements on the atmospheric flow and dispersion processes are discussed in more detail in Section 3.

2.1. ADAPT

The ADAPT model (Sugiyama and Chan, 1998) assimilates data from observations (e.g., from surface stations, rawinsondes and profilers) and/or weather forecast models, as well as land-surface data, for use in the NARAC dispersion model, LODI. ADAPT constructs meteorological fields (mean winds, pressure, precipitation, temperature, turbulence quantities, etc.) based on a variety of interpolation methods and atmospheric parameterizations (Chan and Sugiyama, 1997; Sugiyama and Chan, 1998). ADAPT produces non-divergent wind fields using an adjustment procedure based on the variational principle and a finite-element discretisation. The solution is obtained via conjugate gradient solvers, using a stabilisation matrix to improve computational efficiency.

In emergency response mode, ADAPT is typically run by ingesting real-time observational or numerical weather prediction data. Terrain and atmospheric stability effects are introduced through the variational mass-conservation adjustment process. Atmospheric stability is considered also in other parts of the code to account for its

effects on meteorological fields. Land-surface characteristics and surface heat and momentum fluxes can be used to diagnose horizontally averaged properties of the mean wind and turbulence, using similarity theory relationships. ADAPT diagnostic simulations typically require under a minute to execute on a 2.4-GHz CPU.

ADAPT estimates turbulence quantities required by the dispersion model, LODI, using similarity theory scaling relationships. The methods summarized by van Ulden and Holtslag (1985) can be used to estimate surface heat and momentum fluxes and turbulence scaling parameters (e.g., friction velocity, u_*, Obukhov length, L, convective velocity scale, w_*, and boundary layer depth, z_i) from near-surface meteorological observations and land-use data. The turbulent diffusivities, K_x, K_y and K_z, are calculated as a function of height and horizontal location using these scaling parameters and similarity theory relationships as described by Nasstrom et al. (2000).

2.2. LODI

For regional to global scale atmospheric dispersion, NARAC uses a 3D Lagrangian stochastic, Monte Carlo atmospheric dispersion model that is coupled to ADAPT. The NARAC 3D particle dispersion model LODI simulates the processes of mean wind advection, turbulent diffusion, radioactive decay, first-order chemical reactions, wet deposition, gravitational settling, dry deposition and buoyant/momentum plume rise. Additional terms are used to calculate the production of radionuclides due to the decay of other radionuclides in a decay chain.

The advection-diffusion equation is solved using the Lagrangian stochastic, Monte Carlo method, in which deterministic particle displacements due to the mean wind are calculated using the Runge-Kutta methods described by Leone et al. (1997). The displacement of a particle due to turbulent diffusion is performed using the method developed by Ermak and Nasstrom (2000) based on a skewed, non-Gaussian particle position probability density function, necessary for the efficient simulation of diffusion in inhomogeneous turbulence (especially near the ground surface). Additional details on LODI can be found in Leone et al. (2005).

3. Urban parameterization formulation

In a modeling system such as ADAPT/LODI, dispersion depends on the mean wind, eddy-diffusivities, turbulence, and any initial dispersion that occurs due to the large building-induced eddies or wakes. The dispersion and eddy-diffusivities are described below, whereas the initial dispersion induced by near-source buildings is discussed in Section 5.2.3. In the following, the conceptual and morphological models are adopted from others, whereas the formulations for the near-surface winds, turbulence profiles, and vertical diffusivity are new adaptations or modifications for this urban parameterization.

3.1. Conceptual model

The urban convective boundary layer can be considered to consist of four sublayers starting from the surface and moving upwards: the urban canopy layer (UCL), the roughness sublayer (RSL), the inertial sublayer (ISL), and the "outer" or "mixed" layer (Fig. 1). This is effectively the conceptual model in Grimmond and Oke (2002) with the addition of the outer layer.

In the UCL, the mean wind and turbulence are directly affected by obstacles leading to flow over and around buildings and along street canyons, and in general to a substantially reduced mean wind in comparison to the rural upwind flow. A key length scale for characterizing the urban canopy effects on the mean wind and turbulence is the average building height h. In the next layer—the RSL, the mean wind and turbulence are affected by the individual wakes generated by the buildings. The depth of the RSL may

range from the surface up to 2 to 5 h depending on the variable of interest (e.g., mean wind, turbulent shear stress, or turbulence velocities). Therefore, the RSL layer includes the UCL. Above the RSL lies the ISL, which is a horizontally homogeneous region wherein the mean wind and turbulence are in equilibrium with the underlying surface; here, the ISL is assumed to extend to 10% the height of the boundary layer. In the ISL, the mean wind follows the Monin-Obukhov (MO) similarity profile, and the surface is characterized by the roughness length z_0, the displacement height d, and the surface heat flux. The urban boundary layer (UBL) may also contain an upper or outer layer wherein the mean wind departs from the MO profile; for example, during daytime convective conditions, there will likely be a "well mixed" layer above the ISL.

3.1.1. Morphological parameters

The following are five morphological parameters representing key aspects of the parameterization formulation (which is described in the next four subsections):

- h, the UCL depth, is the grid-cell averaged building height where the average is weighted with each building plan view area. In the urban area of Oklahoma City, Oklahoma (see Section 4), with a grid with horizontal increments of 250 m, the maximum, minimum, average, and standard deviation values of h are 60.3, 4.7, 7.2, and 5.4, respectively.
- h_{rs}, the RSL depth, which in this study is taken as three times h;
- z_0, the surface roughness length;
- d, the displacement height; and

- λ_f, the grid-cell averaged fractional frontal area of buildings; equals to A_F / A_T, where A_F and A_T are the grid-cell averaged frontal and total area of buildings, respectively. The maximum, minimum, average, and standard deviation values of λ_f (over a grid with 250 m increments) are 0.28, 0.003, 0.034, and 0.046, respectively.

The morphological calculations were performed similarly to Burian et al. (2005), using the NARAC Geodata Framework that is based on custom software. The National Geospatial-Intelligence Agency and the Science Applications International Corporation provided in the form of shapefiles the three-dimensional input building data. Several alternative analytical expressions or parameterizations are available for obtaining z_0 and d by morphometric methods, which relate these aerodynamic parameters to the surface morphology — h, λ_f and λ_p (the average fractional plan area); e.g., see Garratt (1992), Grimmond and Oke (1999), MacDonald et al. (1998a), and Hanna and Britter (2000). Grimmond and Oke (1999) give an extensive summary of the methods and evaluate six of them using z_0 and d values from North American cities. There is considerable scatter of the observed values about the predicted z_0 and d for all of the methods; however, given the nature of the observations, this should probably be expected.

In this study, λ_f is approximated by the product of the mean height, breadth, and density of the urban roughness elements, whereas z_0 and d are estimated by the simple rule-of-thumb, $z_0 = 0.1h$ and $d = 0.5h$ (Grimmond and Oke, 1999). The average fractional frontal area λ_f is used in the urban parameterization to account for the drag effects of the building walls on the airflow. Its value changes with wind direction, and in

this study it has been computed for each grid cell for eight different wind directions, each 45° apart from the other.

3.1.2. Wind profile

A key requirement for ADAPT is that the profiles of meteorological variables be continuous functions of height z and all of the other parameters defining the profiles. Here a three-layer model of matching analytical expressions is proposed for parameterizing the mean wind in the urban convective boundary layer. Separate expressions for the UCL, RSL, and ISL are used, but the method ensures that the wind speed is continuous from one layer to the next.

In the ISL ($z > h_{rs}$), the mean wind is given by the MO profile with stability effects included. For the RSL ($h < z < h_{rs}$), we adopt MacDonald's (2000) profile, which is based on neutral flow and is logarithmic in form with a height-dependent diffusivity length scale l_{rz}. The l_{rz} matches the MO value for neutral conditions at $z = h_{rs}$ and the constant scale l_c in the ULC at $z = h$. In the UCL ($z < h$), the mean wind is given by an exponential profile (MacDonald, 2000). In the parameterization, the wind speed is continuous with height, whereas the wind gradient (du/dz) changes at the layer interfaces. Adoption of a more general RSL model that maintains a continuous du/dz and includes stability effects is a subject for future work.

A summary of the profiles and required parameters to determine them are as follows:

$$u(z) = \frac{u_*}{k}\left[\ln\left(\frac{z-d}{z_0}\right) - \Psi\left(\frac{z-d}{L}\right)\right] \quad z \geq h_{rs} \text{ (ISL)} \qquad (1)$$

$$u(z) = \frac{u_*}{b_1} \ln\left(\frac{l_{rz}}{l_{rs}}\right) + u_{rs} \quad h < z < h_{rs} \text{ (RSL)} \tag{2}$$

$$u(z) = U_h \exp\left[\gamma\left(\frac{z}{h} - 1\right)\right] \quad z < h \text{ (UCL)} \tag{3}$$

where,

$$u_{rs} = \frac{u_*}{k}\left[\ln\left(\frac{h_{rs} - d}{z_0}\right) - \Psi\left(\frac{h_{rs} - d}{L}\right)\right] \tag{4}$$

$$b_1 = \frac{1}{h_{rs} - h}\left[k(h_{rs} - d) - l_c\right] \tag{5}$$

$$l_{rz} = l_c + b_1(z - h) \tag{6}$$

$$l_{rs} = k(h_{rs} - d) \tag{7}$$

$$l_c = h\left(\frac{\overline{C_{DH}}\lambda_f\left(1 - \exp(-2\gamma)\right)}{4\gamma^3}\right)^{1/2} \tag{8}$$

$$\gamma = a_1\lambda_f \tag{9}$$

$$U_h = \frac{u_*}{b_1} \ln\left(\frac{l_c}{l_{rs}}\right) + u_{rs} \tag{10}$$

and where u is the wind speed, z is the vertical coordinate, u_* is the friction velocity, k is the von Karman's constant (equal to 0.4), Ψ is a stability function (Dyer and Hicks, 1970), L is the MO length, b_1 is a multiplicative factor, C_{DH} is an average drag coefficient in the canopy (equal to 1.2), and a_1 is an empirically derived constant equal to 9.6, based on wind tunnel experiments over cube arrays (MacDonald, 2000). The l_{rz} is the height-dependent length scale in the RSL, l_{rs} is the length scale at the top of the RSL, l_c is the vertically-averaged length scale in the UCL, γ is the "attenuation" or decay coefficient in

the exponential profile, U_h is the wind speed at the top of the UCL, and u_{rs} is the wind speed at the top of the RSL.

We note that MacDonald (2000) solves for h_{rs} by equating the RSL and ISL (or MO) wind profiles at $z = h_{rs}$, but this solution is quite sensitive to z_0 and could vary substantially with small changes in z_0. We prefer to avoid that situation and thus, we specify h_{rs} independently by assuming it will be given or parameterized as some factor times h; we choose $h_{rs} = 3h$.

The above analytical profiles can be computed once the u_*, u_{rs}, and U_h are determined. We compute u_* and L using the sensible heat flux (see Section 3.1.5) within an iterative procedure similar to the one used in Perry (1992).

3.1.3. Turbulence velocity variances

The turbulence velocity variance (σ^2) parameterizations are given for heights above as well as within the canopy. Above the canopy, the velocity variances are assumed to follow the ADAPT expressions (Nieuwstadt, 1985; Lenschow et al., 1988; Rodean, 1996) with urban effects incorporated through the use of "urban" values of u_* (previous section), boundary layer height z_i (Section 3.1.5), and the introduction of h, which serves as the zero-plane reference height. This results in

$$\sigma_v^2 = Au_*^2\left[1-(z-h)/(z_i-h)\right]^{3/2} \quad (h < z < z_i) \tag{11}$$

$$\sigma_w = 1.3u_*\left[1-(z-h)/(z_i-h)\right]^{3/4} \quad (h < z < z_i) \tag{12}$$

for neutral and stable conditions, and

$$\sigma_v^2 = Au_*^2\left[1-(z-h)/(z_i-h)\right]^{3/2} + Bw_*^2 \quad (h < z < z_i) \tag{13}$$

$$w_*^3/u_*^3 = -z_i/kL \tag{14}$$

for convective conditions, where A is a constant (equal to 4.25), B is a constant (equal to 0.34), and w_* is the convective velocity scale; see Sugiyama and Chan (1998) for the ADAPT formulation. Here *u*, *v*, and *w* components are in the three Cartesian directions. In addition, we assume that $\sigma_u = \sigma_v$. These expressions account for both shear-generated turbulence through the terms involving u_* and buoyancy-generated turbulence through the term involving w_* (Eq. 13). When h = 0, the original ADAPT expressions are recovered.

3.1.4. Vertical eddy diffusivities

LODI models turbulence dispersion via a random walk method that uses atmospheric eddy diffusivity (K) values to parameterize the effects of turbulent motions that are unresolved by the gridded mean winds. K_x, K_y, and K_z are the eddy diffusivities for the three coordinate directions (the eddy diffusivity tensor is assumed to be diagonal). The K_z used in ADAPT/LODI for non-urban conditions can be written as,

$$K_z = K_{z1}(z) f_3(z/z_i) \tag{15}$$

where

$$K_{z1} = \frac{u_s l_s(z)}{\phi_h(z/L)} \tag{16}$$

and

$$f_3 = \exp\left(\frac{-4z}{z_i}\right) \tag{17}$$

u_s is the diffusivity velocity scale $u_s = u_*$, l_s is the scalar length scale equal to kz, and Φ_h is the MO dimensionless temperature gradient function. The K_{z1} is the MO diffusivity in the atmospheric surface layer (e.g., Garratt, 1992) and when multiplied by f_3 (Eq. 15) gives an appropriate K_z throughout the entire boundary layer.

We assume that the maximum stress $-u_*^2$ occurs at $z = h$, i.e., for a UCL with a uniform or constant building height as in the direct numerical simulations of Coceal et al. (2006). Thus, we neglect any stress variation within the RSL consistent with the MacDonald (2000) mean wind model as presented in Section 3.1.2.

For the UBL, we first consider modifications to the K_{z1} for neutral conditions or $\Phi_h = 1$. The u_s and l_s are parameterized separately with u_s given by:

$$u_s = \frac{\sigma_w}{c_w} \quad z < h \tag{18}$$

$$u_s = u_* \quad z \geq h \tag{19}$$

where $c_w = 1.3$, as in Eq. (12). Eq. (18) accounts for the decreased σ_w in the UCL but requires u_s to match or equal u_* at $z = h$, whereas Eq. (19) is consistent with the existing ADAPT formulation.

The expressions for the length scale l_s are guided in part by the parameterization in MacDonald (2000) and by measured turbulence length scales (the vertical component) found in plant canopies (Raupach et al., 1996; Fig. 1i in Finnigan, 2000). The l_s is given by the following:

$$l_s = l_c \quad z < d \tag{20}$$

$$l_s = l_c + \frac{z-d}{h_f - d}\left[k\left(h_f - d\right) - l_c\right] \quad d \le z < h_f \tag{21}$$

$$l_s = k\left(z - d\right) \quad h_f \le z \tag{22}$$

330 In Eq. (21), a linear variation of l_s with z occurs between d and a height h_f, which is empirically determined to be in the range $h < h_f < 1.5h$ based on the data in Finnigan (2000). We assume $h_f = h$. The K_{z1} resulting from the above u_s and l_s is continuous in z.

The modified expression for K_z is completed by including ϕ_h and $f_3(z)$ in the following forms:

335 $$\phi_h = 1 \quad z < d \tag{23}$$

$$\phi_h = \phi_h\left(\frac{z-d}{L}\right) \quad z \ge d \tag{24}$$

and

$$f_3 = 1 \quad z < d \tag{25}$$

$$f_3(z) = \exp\left[-4\frac{z-d}{z_i - d}\right] \quad z \ge d \tag{26}$$

340 Equation (24) is the conventional adaptation of MO theory to canopies and is expected to be conservative, i.e., lead to higher predicted-than-observed concentrations, because the observed Φ_h ($\Phi_{h,obs}$) just above a canopy is typically 1/2 to 2/3 of the MO values (Raupach and Thom, 1979; Weil and Massman, 1996) and hence $K_{z,obs} \ge K_{z,MO}$ (where $K_{z,obs}$ is the observed K_z and $K_{z,MO}$ is the K_z resulting from MO theory) as indicated by

345 Eq. (16) above. This conservative approach for K_z is considered appropriate as an "initial" or "baseline" dispersion model for emergency response applications but may need future modification based on the results below.

3.1.5. Boundary Layer height and heat fluxes

Daytime convective mixing heights were estimated using the modified Carson method (Carson, 1973) employed by the AERMET model (Cimorelli et al., 2005). We modified the AERMET code to allow the user to supply values for the ratio of the surface heat flux to the net radiation in order to more accurately calculate the energy balance over specific land use types. The sensible heat flux is then computed as in Simpson et al. (2007). Convective mixing heights are estimated from the modified Carson method using the daytime integrated heat flux and the potential temperature profile from an early morning sounding.

3.2. Effects of urban parameterization on velocity variances and wind speed profile

Fig. 2 shows an example of the effect of the urban parameterization on the vertical profiles of the horizontal turbulence velocity variances (left panel) and wind speed (right panel) for the second release of the fourth intensive operating period (IOP) of the Joint Urban 2003 field campaign (see next section). Note that only one model curve is shown for the urban (URB) and rural (RUR) cases since it is assumed that $\sigma_u = \sigma_v$ in the parameterization. The values from the run with and without the parameterization are in blue and red, respectively. Qualitatively the urban parameterization more closely replicates the vertical profiles as measured at a crane (values in black) operated by LLNL during the field campaign. The crane was located (green triangle in Fig. 3) approximately 750 m North (typically downwind) of the CBD. For this case, both runs tend to

underestimate the velocity variances above 20 m. However, the run with the new urban parameterization is considerably closer to the observed values, capturing the increased turbulence induced by the presence of the buildings. For the wind speed profile, the urban parameterization produces values close to the measurements between 15 and 70 m, while under-predicting the speed between 10 and 15 m. In contrast, the rural parameterization consistently over-predicts the observed values. The effect of the urban parameterization is to produce reduced winds everywhere except close to the surface. The exponential shape of the bottom part of the urban wind speed profile, which results from the implementation of equation (3) in the UCL should also be noted. An in-depth analysis of the parameterization performance for the meteorological variables will be presented in a follow-up paper. In the following, the focus is on the skill of the parameterization in replicating the observed concentrations (Section 5).

4. Joint Urban 2003 and simulations set up

385

4.1. Joint Urban 2003

During the summer of 2003, from 28 June to 31 July, a series of tracer gas sulfur hexafluoride (SF_6) releases were made in downtown Oklahoma City, Oklahoma (Allwine
390 et al. 2004) as part of a major urban study, the Joint Urban 2003 (JU03), that included a variety of meteorological and dispersion measurements. The Journal of Applied Meteorology and Climatology recently published a special issue dedicated to JU03 (Volume 46, Issue 12), including several contributions based on JU03 and advancements of our understanding of the urban boundary layer.

395 Oklahoma City is situated on flat terrain and grasslands in the Great Plains. Summertime winds are typically from the south and the average surface wind speed for the month of July is 5.1 m s^{-1}. This field study was conducted in the CBD of Oklahoma City, which includes the tallest buildings in the city as well as several shorter buildings. Oklahoma City is a typical medium-size U.S. city, with the tallest building being about
400 150 m tall. The CBD contains two other buildings that are at least 120 m tall, and eight additional buildings that are between 75 and 120 m tall. Other buildings in downtown Oklahoma City are less than 50 m, with many structures about 15 m tall.

The urban parameterization presented here has been designed to represent the urban convective boundary layer. With different stability regimes the conceptual model
405 presented in Section 3.1 (Fig. 1) may not be appropriate, e.g., in a stable nocturnal

boundary layer the ISL may be non-existent. Here the parameterization is tested only for daytime, convective conditions. Data from three IOPs, each involving three 30-min daytime releases of sulfur hexafluoride (SF_6), have been used to evaluate the performance of the urban parameterization. Following the start of each release, two hours of sampler monitoring concentration were available. Ground-based samplers were located at 3 m above ground level (AGL), with 55 samplers in the CBD, referred herein after also as "urban core", 23 samplers over an arc 1 km downwind of the source location, 21 at a 2 km arc, and 21 on a 4 km arc (Fig. 3). General information on IOPs 2, 3 and 4 is summarized in Table 1 and more details can be found in Allwine et al. (2004).

4.2. Simulation set up

In this study, we tested a new urban parameterization for a fast-response modeling system for emergency response applications. The simulation has been set-up similarly to the conditions of an emergency response for an accidental or deliberate atmospheric release in Oklahoma City. Fig. 4 shows the locations of the five surface stations and upwind profiles that were assimilated to diagnose the meteorological field. Quantities measured include wind speed and direction, pressure, temperature and dew point, and cloud cover fraction. Upper air observations of wind speed and direction were available at the Norman airport (KOUN) located about 25 km upwind of the Oklahoma City CBD. The surface stations were located between 10 and 60 km around the city, as illustrated in Fig. 4. The dispersion simulation was conducted using 100,000 marker particles. The horizontal grid increments used in the experiments are 125, 250, 500 and 1000 m, while

there are a total of 38 vertical levels, among which 7 are in the first 20 m AGL, and 16 in the first 100 m.

The following is the overall sequence of the calculations. First ADAPT blends the available observations (both surface and upper air soundings) to the three dimensional grid. This is performed via a combination of interpolation and extrapolation techniques, including both direct and iterative solvers and atmospheric parameterizations (for details see Sugiyama and Chan, 1998). Then the u_* and L are computed from the ISL profile (Eq. 1) using the wind speed from the diagnosed wind field at $z = 0.1z_i$ and the sensible heat flux (see Section 3.1.5) with an iterative procedure similar to the one used in Perry (1992). For a sufficiently deep convective boundary layer ($h << z_i$), it is assumed that the rural and urban wind speeds are approximately the same at and above the surface layer top ($0.1z_i$), i.e., in the mixed or outer layer. Given the u_* and L the urban parameterization is applied to correct the mean wind profile (below $0.1z_i$), the turbulence velocity variances, and the vertical eddy diffusivity as discussed in Section 3. Sensitivity tests on the effect of different values of the matching wind speed height (spanning ± 30% of $0.1z_i$) produce small differences in the results (not shown).

5. Results

This section presents qualitative and quantitative comparisons of observations and predictions. The runs of the prediction system without the urban parameterization are referred to hereinafter as RUR (i.e., rural, with a roughness length of 0.1 m), while the runs with the parameterization turned on are indicated as URB (i.e., urban). Both observed and predicted concentrations are 30-min averages.

5.1. Qualitative analysis

The left panel of Fig. 5 shows the 10^{-8} g m^{-3} isosurface of the RUR prediction, while the right panel shows the same isosurface from the URB runs, for the second release of IOP3, with the model run with 250 m grid increments with the wind as indicated. The source is located just upwind of the concentration isosurface.

The URB plume is broader both horizontally and vertically, particularly in the near source region. This is qualitatively consistent with a daytime release in urban environments where the presence of buildings is expected to enhance both vertical and lateral mixing when compared to a similar release in rural settings. Fig. 6 includes two 30-min average concentration isosurfaces (10^{-8} g m^{-3} in red and 10^{-7} g m^{-3} in blue) and in this case the wind is coming out of the figure plane. The left panel shows isosurfaces resulting from the RUR run, while the right panel from the URB run, both performed with 250 m grid increments. The results show that the higher concentration region (dark blue isosurfaces) is extended much further downwind for the RUR run than for URB.

This can be understood in terms of a simple Gaussian plume model, with the plume centerline concentration given by $C \propto Q/(u\sigma_y\sigma_z)$, where Q is the source emission rate, u is the plume mean wind speed, and σ_y, σ_z represent the plume lateral and vertical root-mean-square dispersions or spreads. From the above proportionality, the ratio of the rural to urban concentration (denoted by subscripts r and u) is $C_r/C_u = u_u\sigma_{yu}\sigma_{zu}/(u_r\sigma_{yr}\sigma_{zr})$ at a given downstream distance. Beyond the CBD, the results show that $C_r/C_u > 1$ but the wind speed ratio u_u/u_r is <1. Therefore, the enhanced dispersion due to the urban roughness must be more than sufficient to offset the effects of the wind speed. That is, we must have $\sigma_{yu}\sigma_{zu}/(\sigma_{yr}\sigma_{zr}) > u_r/u_u$ at a given downwind distance. This inequality can be further understood in terms of the residence time or time for the material to travel across the city, which is greater for the URB than for the RUR due to reduced wind speed (u_u). The higher residence time allows for greater diffusion of material outward or away from the plume centerline, thus creating a larger plume cross section. Evidence of an enhanced cross section (at least in the y or lateral direction) can be seen in Figs. 7 (at 16:30 UTC / 11:30 local time, 7 July 2003) and 8 (at 17:00 UTC / 12:00 local time, 7 July 2003), which show plan views of the predicted concentration (contours) and the sensor measurements (circles) during the first release of IOP3, as provided by runs with 250 m grid increments. The panels on the left are the RUR runs, while the panels on the right are the URB runs. Although both URB and RUR appear to be over predicting the measurements in the urban core, URB is closer to the observations. For example, in the RUR case (left panel of Fig. 7), the high concentration cloud is rapidly advected beyond the CBD, resulting in a largely

overestimated concentration in the urban core, as well as at the first (1 km) downwind arc. The URB runs appear to represent better qualitatively the lateral spread of the plume, particularly at the downwind arcs (1, 2 and 4 km). Similar patterns were observed for other times and IOPs (not shown).

5.2. Quantitative comparisons

This subsection presents a quantitative comparison between observations and predictions based on several metrics. The statistics are computed by clustering together the three releases of the three IOPs. The parameterization performance is analyzed by running the modeling system for four grids with different horizontal grid increments, i.e., 125, 250, 500 and 1000 m, to observe the effect of spatial averaging (on building parameters, meteorological variables, and concentration values) at different scales. For a selected grid increment (250 m), further analysis is carried out by examining additional metrics to estimate other aspects of the performance of the new urban dispersion modeling system. Finally, it is shown how the parameterization performance can be further improved by representing the urban point source release by a Gaussian geometry with initial x, y and z spreads.

5.2.1. Overall performance and sensitivity to different grid increments

The Taylor diagram (Taylor, 2001) is used to create a multi-statistics plot of Pearson product-moment coefficient of linear correlation (herein "correlation"), centered root

mean square error (CRMSE) (computed by pairing observations and predictions in time and space), and normalized standard deviation (NSD), defined as follows:

$$correlation = \frac{\sum_{i=1}^{N_{point}} \{[C_o(i) - \overline{C_o}][C_p(i) - \overline{C_p}]\}}{\sqrt{\sum_{i=1}^{N_{point}} [C_o(i) - \overline{C_o}]^2 \sum_{i=1}^{N_{point}} [C_p(i) - \overline{C_p}]^2}} \quad (27)$$

$$CRMSE = \sqrt{\frac{1}{N_{point}} \sum_{i=1}^{N_{point}} [(C_p(i) - \overline{C_p}) - (C_o(i) - \overline{C_o})]^2} \quad (28)$$

$$NSD = \frac{\sqrt{\frac{1}{N_{point}} \sum_{i=1}^{N_{point}} [(C_p(i) - \overline{C_p})]^2}}{\sqrt{\frac{1}{N_{point}} \sum_{i=1}^{N_{point}} [(C_o(i) - \overline{C_o})]^2}} \quad (29)$$

where N_{point} is the number of valid observation/prediction pairs of 30-min average concentrations, C_p is the model prediction, C_o is the observed concentration, and the bar above the quantity denotes the average over a group of sensors. Figs. 9, 10, 11 and 12 show Taylor diagrams for the runs with 125, 250, 500, and 1000 m grid increments, respectively. The arrow tails represent the statistics of the RUR runs, while the arrow heads represent the URB runs. The red square on this diagram represents the observations. CRMSE is the distance on the diagram between the point representing the forecast and the red square representing the observations. If the arrow points toward to the observation it means the urban parameterization is correcting the forecast statistically in the right direction, by reducing the CRMSE.

To better understand the parameterization performance, the above metrics have been computed by grouping the concentration sensors as follows:

- all the sensors together (black arrow, N_{point} equal to 1104),
- the sensors in the urban core (green arrow, N_{point} equal to 637),

- and the sensors at the three downwind (1 km, 2 km, and 4 km) arcs (light blue, magenta, and blue arrows, and N_{point} equal to 202, 146, and 125, respectively).

Applying a sampling uncertainty of $1/\sqrt{N_{point}}$ for all sensors together, the CBD sensors, and the sensors at the three downwind arcs, yields 3%, 4%, 7%, 8% and 9%. This means that most of the differences between the reported values of the statistical metrics have a statistical significance at the 95% confidence interval.

This grouping allows us to estimate the overall prediction skill, and to see how the skill varies spatially. The modeling system used in this study is not building-aware, but instead captures the average effects of the urban roughness elements on the atmospheric flow and dispersion processes. Therefore, since the sensors in the urban core are located for the most part in deep street canyons, it is expected to be challenging for the ADAPT/LODI models which do not resolve individual buildings to closely replicate the concentrations measured by this group of sensors. As discussed below, such a performance is significantly affected by the grid increments at which the modeling system is run.

In all cases the arrows either point closer toward the point representing the observations, or the arrow tail and head are at a similar distance from it. This means that the runs with the urban parameterization lead to improvements (often significant) of the prediction quality as measured by these statistics in almost all cases. The only cases where the URB runs do not produce an improvement in prediction skill are for the 1000 m grid increments for the cases representing all the sensors and the sensors in the CBD.

At the downwind arcs the performance improvement of URB with respect to RUR increases going from 1000 m grid increments (Fig. 12) down to 250 m grid increments

(Fig. 10). The 250 and 500 m (Fig. 11) URB runs are the ones with the better statistics, meaning that for JU03 the new urban parameterization is more skillful at these grid increments; there is some performance degradation with the 125m grid (Fig. 9). The above results cannot be generalized, and different cities with different building morphologies may require different grid increments to attain optimal performance.

Noticeably, the largest improvements (i.e., longer arrows) are observed for the sensors at the first and second arc. Improvements for the third arc (particularly with 250 and 500 m increments) are not as pronounced as at the first and second arc. This implies that for the Oklahoma City IOPs analyzed here the effect of the roughness elements starts to vanish 4 km downwind (i.e., at the third arc). The statistics computed with all the sensors and with only the sensors in the urban core are very similar, because the concentrations (both predicted and observed) are much higher in the urban core than at the downwind arcs. It is interesting that the best performance of the URB runs for these two groups of sensors is obtained with 1000 m grid increments, and this performance monotonically decreases with reduced grid increments. This is due mainly to the fact that the runs with larger grid increments result in concentration distributions with a much lower NSD than runs with finer grids, bringing the model standard deviation closer to the observed values. For these groups of sensors, the correlation values are similar across runs with different grid increments. The overall result is a better (lower) CRMSE with 1000 m increments, as shown by the green and black arrow tails and heads being closer to the observations (red square) than with the finer grid spacing. The CRMSE increases with a reduction in grid increments.

The Taylor diagram provides a statistical summary of the degree of pattern correspondence between the predictions and observations (Taylor, 2001). However, to have a full picture of the prediction skill, the prediction bias also needs to be evaluated. Bias is defined as the "difference of the central location of the forecasts and the observations" (Jolliffe and Stephenson, 2003). In this study we have computed the fractional bias (FB), as follows:

$$FB = \frac{\left(\overline{C}_p - \overline{C}_o\right)}{0.5\left(\overline{C}_p + \overline{C}_o\right)} \tag{30}$$

The closer the FB values are to 0 the better the predictions; positive FB values mean an over-prediction, whereas negative values indicate an under-prediction. Since FB is a normalized metric, it allows estimating the bias for different groups of sensors without having the results affected by the different magnitude of predicted and observed concentrations, e.g., in the urban core and at the downwind arcs.

Fig. 13 shows FB values computed with data from the three IOPs for the five groups of sensors used in the previous analysis (all, urban core, first, second and third arc), and for the four grid increments (1000, 500, 250, and 125 m). For each of those, the left bar represents the FB of the RUR run, while the right bar is for the URB run.

The URB runs reduce the bias, often drastically, except for the cases of all sensors, the urban core, and the third arc for the 1000 m increment runs. FB values decrease from the urban core to the downwind arcs, and at the three arcs, the FB decreases with grid increments from 1000 to 250 m, whereas at 125 m, the FB values are higher than at 250 m. This confirms what was shown in the Taylor diagrams, i.e., the parameterization performance peaks at the 250 m grid increment.

5.2.2. Measure of effectiveness

Warner et al. (2004) introduced the measure of effectiveness (MOE), defined as:

$$MOE = (x, y) = \left(\frac{A_{OV}}{A_{OB}}, \frac{A_{OV}}{A_{PR}} \right) = \left(1 - \frac{A_{FN}}{A_{OB}}, 1 - \frac{A_{FP}}{A_{PR}} \right) \quad (31)$$

where A_{OV} is the area of overlap between the prediction and the observation, A_{OB} is the area of the observation, A_{PR} is the area of the prediction, A_{FN} is the area of false negative (zero prediction but non-zero observation), and A_{FP} is the area of false positive (non-zero prediction but zero observation). This two-dimensional area-based metric includes information about the shape and size of the predicted and observed plumes, as well as directional effects. The perfect MOE is (1, 1), and is obtained when there is complete overlap of the predicted and observed plumes. MOE values on the 1:1 line indicate that the observed and predicted plumes have the same area, even though their locations may be different. As explained by Warner et al. (2004), MOE can be computed when the available predictions and observations are paired in space and time, as for JU03, without the need to have the actual physical areas described above.

In Fig. 14, x and y as defined in Eq. (31) are plotted on the abscissa and ordinate, respectively. An increasing value of x corresponds to a decreasing number of false negatives, whereas an increasing value of y indicates a decreasing number of false positives. We compute the MOE for the 250 m predictions by grouping the sensors as in the previous analysis. The RUR run values are shown with open squares, while the solid squares correspond to MOE values associated with the URB runs. In all cases, the MOE values of the URB runs are closer to the 1:1 line and the (1, 1) point, meaning that the urban parameterization produces a plume that overlaps better and covers an area closer to

the observed one by comparison to the RUR runs. The urban parameterization reduces false positives, with the greatest improvements occurring at the first and second arcs. The best MOE value is obtained at the third arc (4 km downwind of the source location) for both the URB and the RUR runs implying good overlap of the predicted and observed areas and that at that distance the effect of the city on the atmospheric flow is less pronounced that at the other two sensor arcs or in the CBD. Note that for URB, the false positive for "all sensors" is about 0.35, whereas the false negative is about 0.65, meaning that there is more overprediction than underprediction; this is consistent with a positive FB (= 0.4, all sensors) shown in Table 2.

5.2.3. Urban source geometry

For sources in the UCL, enhanced initial spread of a plume has been observed in early field studies (McElroy and Pooler, 1968), dispersion experiments with idealized block arrays both outdoors (Davidson et al., 1995; MacDonald et al., 1997, 1998b) and in laboratory settings (Davidson et al., 1996; MacDonald et al., 1998b), and in simulations with high-resolution building-aware modeling approaches (e.g., see Fig. 12 in Chow et al., 2008 for IOP3 of JU03). The enhanced lateral and vertical dispersion occurs due to building-induced eddies and wakes, plume splitting about obstacles, and wind direction variability.

Since ADAPT/LODI cannot model the effects of individual buildings critical to resolve the initial distribution, an empirical urban source term is needed. The initial dispersion is a non-diffusive phenomenon—i.e., not based on a "small eddy" or eddy-

diffusion approach—due to the locally large eddies with large time scales. This can be modeled by a probability density function type model (Weil, 1996), which is consistent with Taylor's (1921) short-time statistical theory, or it can be addressed by including an initial dispersion. In the following, the second approach is proposed.

To account for this initial spread, a simple objective approach suitable for emergency response applications has been adopted. The point source release of each IOP has been represented with a Gaussian geometry with initial mean-square spreads of $\sigma_{x_0}^2$, $\sigma_{y_0}^2$, and $\sigma_{z_0}^2$ describing the initial particle distribution. These spreads are chosen as the variance of the building dimensions in the three Cartesian directions in the domain cell where the source is located. Although a more appropriate approach would be to consider only the dimensions of the downwind near-source buildings, the simple solution adapted here can be easily implemented in operational settings to produce fast response dispersion predictions as in NARAC.

Table 2 shows the FB, correlation, and normalized standard deviation calculated for the five sensor groups, by representing the source either as a point source (as in the results presented in Sections 5.2.1 and 5.2.2) or as a Gaussian source as described above. Accounting for the initial spread significantly reduces the fractional bias and improves the correlation, particularly when computing the statistics with the sensors in the urban core (and therefore also when all the sensors are used to compute the statistics). For the other groups of sensors at the downwind arcs, the metrics are essentially the same. Accounting for the initial spread with a Gaussian geometry of the source allows the predicted plume to more closely resemble what happens outdoors, where the turbulence induced by the building near the source substantially dilutes the released contaminant,

leading to concentrations (when averaged over 30-min) lower than they would be otherwise without the near-source buildings.

5.2.4. Comparison with other models

The performance of the urban parameterization has been compared with the skill of other urban modeling systems with similar or greater complexities that have been tested with the JU03. These systems include the CFD model presented in Chan and Leach (2007), the fast-running building-aware urban dispersion model as in Hendricks et al. (2007) and the dispersion prediction system tested by Warner et al. (2008). The results of this comparison are shown in Table 3. In doing this comparison it is worthwhile to mention that these models are not initialized with the same meteorological data, and that the parameterization introduced in this paper has been tested with limited input data, to replicate real-time emergency response conditions (Section 4.2). Moreover, the statistics shown in Table 3 have been computed with the sensors located in the CBD (with the exception of Warner et al. 2008), and as shown in Section 5.2 this is not the group of sensors where the new urban parameterization should perform best. Nonetheless, the values of the metrics summarized in Table 3 show that the new parameterization has a performance similar to other models.

6. Summary and conclusions

A new urban parameterization capable of producing accurate dispersion predictions in a timely manner for emergency response applications has been presented. The parameterization is designed for the urban convective boundary layer. The modeling system includes the Atmospheric Data Assimilation and Parameterization Techniques (ADAPT) model and the Lagrangian Operational Dispersion Integrator (LODI) model. ADAPT and LODI were developed by the National Atmospheric Release Advisory Center (NARAC) at Lawrence Livermore National Laboratory for operational emergency response predictions (Nasstrom et al., 2007). The parameterization is based on a conceptual model with four sublayers, in each of which the vertical profile of wind, velocity variances, and vertical eddy diffusivity are modified to capture the urban roughness effects on the atmospheric flow in the boundary layer. The formulation has five key parameters: the weighted grid-cell averaged building height (h), fractional frontal area of buildings, the roughness sublayer depth, the surface roughness length, and the displacement height.

ADAPT/LODI performance was tested with concentration data from a major urban study, the Joint Urban 2003 (JU03), that included a variety of meteorological and dispersion measurements taken downtown and downwind of Oklahoma City, Oklahoma (Allwine et al., 2004). To ensure that the new parameterization would be tested in a setting similar to operational conditions, only meteorological data that would be available during NARAC daily operations were used. These include five surface stations distributed around the city (from 10 to 60 km from the release locations) and upper air

data available at the Norman airport about 25 km upwind of the central business district (CBD).

The performance of the new parameterization has been tested with data from three intensive operating periods (IOPs), each including three daytime releases in slightly unstable to unstable conditions. The degree of correspondence (via Taylor diagrams, Taylor, 2001), fractional bias (FB), and the measure of effectiveness (MOE, Warner et al., 2004) have been used to estimate the agreement between predictions and observations. Simulations with the urban parameterization significantly improve the prediction skill as measured by all of the above metrics. The best performance is observed at the downwind arcs (1, 2 and 4 km), since this modeling approach does not explicitly resolve buildings and therefore better captures the average effects of the buildings on the atmospheric flow at these locations. Fractional bias values range from 0.13 to 0.4, correlation values from 0.45 to 0.71, and the centered root-mean-square error is reduced more than 50% in most cases. The performance in the CBD was further improved (i.e., lower biases and higher correlations values) by representing the initial spread induced by near-source buildings with an initial Gaussian distribution. The modeling system has been tested with 125, 250, 500 and 1000 m grid increments, performing best at 250 and 500 m. Although this is an indication of the spatial scales to which the parameterization is better suited, the results cannot be generalized to other cities and meteorological conditions. Moreover, the performance of the new urban parameterization has been compared with the skill of other urban modeling systems with similar or greater complexity, which have been tested with the JU03 (Chan and Leach, 2007; Hendricks et al., 2007; Warner et al., 2008), showing similar prediction skills.

Future development of this approach will include a formulation for nighttime stable conditions and improved representation of winds and diffusivities in the roughness sublayer for all stabilities. Additional improvements in the urban parameterization may be achieved by accounting for wind direction changes and plume channeling induced by the street canyons, which may be important at times as shown by Flaherty et al. (2007a).

Acknowledgments

Field data provided by the following Joint Urban 2003 (JU03) participants were invaluable for this research effort: NOAA/ARL/FRD, VOLPE, LBNL, WSU, UU, DPG, ANL, and PNNL. We are thankful to Steven Hanna (of Harvard School of Public Health) for helpful discussions on JU03 and fast-running modeling applications in urban environments. We thank John Leone (of LLNL) for his earlier effort to develop an urban parameterization for the ADAPT/LODI modeling system, that greatly facilitated the work presented here. We are grateful to Carol Makowski (of NCAR) for proof-reading a version of this paper. Reviews by Gayle Sugiyama (of LLNL) and Alberto Martilli (of CIEMAT) were valuable in strengthening the paper. We are also thankful to Hoyt Walker (of LLNL) for preparing all the urban morphological data used in this study, and to Julie Lundquist (of LLNL) for providing data collected at the crane. This work was performed under the auspices of the U.S. Department of Energy by Lawrence Livermore National Laboratory under Contract DE-AC52-07NA27344.

References

Arya, S. P., 2001. Introduction to micrometeorology. Academic Press, 415 pp.

Allwine, K. J., Leach, M. J., Stockham, L. W., Shinn, J. S., Hosker, R. P., Bowers, J. F., Pace, J. C., 2004. Overview of joint urban 2003—An atmospheric dispersion study in Oklahoma City. Symposium on Planning, Nowcasting and Forecasting in the Urban Zone, Seattle, WA, American Meteorological Society, CD-ROM, J7.1 <http://ams.confex.com/ams/84Annual/techprogram/paper_74349.htm>.

Bornstein, R. D., 1975. Two-dimensional, non-steady numerical simulations of nighttime flows of a stable planetary boundary layer over a rough warm city. Journal of Applied Meteorology 14, 1459–1477.

Brown, M. J., 2004. Urban dispersion—Challenges for fast response modeling. Preprints, Fifth Conference on the Urban Environment, Vancouver, BC, Canada, Amer. Meteorological Society, J5.1.

Burian, S., San, W. S., Brown, M., 2005. Morphological analyses using 3D building databases: Oklahoma City. Report LA-UR-05-1821, Los Alamos National Laboratory, Los Alamos, NM.

Carson, D. J., 1973. The development of a dry inversion-capped convectively unstable boundary layer. Quarterly Journal of Royal Meteorological Society 99, 450467.

Chan, S. T., Sugiyama, G., 1997. A new model for generating mass-consistent wind fields over continuous terrain. Preprint, ANS Sixth Topical Meeting on Emergency Preparedness and Response, San Francisco, CA, 375–378.

780 Chan, S. T., Leach., M. J., 2004. Large eddy simulations of an Urban 2000 experiment with various time-dependent forcing. AMS Fifth Symposium on the Urban Environment, Vancouver, Canada, August 23-27, 2004.

Chan, S. T., Leach, M. J., 2007. A validation of FEM3MP with Joint Urban 2003 data. Journal of Applied Meteorology and Climatology 46, 2127-2146.

785 Chow, F. K., Kosovic, B., Chan, S., 2008. Source inversion for contaminant plume dispersion in urban environments using building-resolving simulations. Journal of Applied Meteorology and Climatology 47, 1553-1572.

Cimorelli, A.J., Perry, S. G., Venkatram, A., Weil, J. C., Paine, R. J., Wilson, R. B., Lee, R. F., Peters, W. D., Brode, R. W., 2005. AERMOD: A dispersion model for

790 industrial source applications. Part I: General model formulation and boundary layer characterization. Journal of Applied Meteorology 44, 682--693.

Coceal, O., Thomas, T. G., Castro, I. P., Belcher, S. E., 2006. Mean flow and turbulence statistics over groups of urban-like cubical obstacles. Boundary-Layer Meteorology 121, 491-519.

795 Davidson, M. J., Mylne, K. R., Jones, C. D., Phillips, J. C., Perkins, R. J., Fung, J. C. H., Hunt, J. C. R., 1995. Plume dispersion through large groups of obstacles--a field investigation. Atmosheric Environment 29, 3245-3256.

Davidson, M. J., Snyder, W. H., Lawson, W. E., Hunt, J. C. R., 1996. Wind tunnel simulations of plume dispersion through groups of obstacles. Atmosheric

800 Environment 30, 3715--3731.

Dyer, A. J., Hicks, B. B., 1970. Flux-gradient relationships in the constant flux layer. Quarterly Journal of the Royal Meteorological Society 96, 715—721.

Ermak, D., Nasstrom, J., 2000. A Lagrangian stochastic diffusion method for inhomogeneous turbulence. Atmospheric Environment 34, 1059-1068.

Finnigan, J. J., 2000. Turbulence in plant canopies. Annual Review of Fluid Mechanics 32, 519–571.

Flaherty, J., Lamb, B., Allwine, K. J., Allwine, E., 2007a. Vertical tracer concentration profiles measured during the Joint Urban 2003 dispersion study. Journal of Applied Meteorology and Climatology 46, 2019-2037.

Flaherty, J., Stock, D., Lamb, B., 2007b. Computational fluid dynamic simulations of plume dispersion in urban Oklahoma City. Journal of Applied Meteorology and Climatology 46, 2010-2126.

Garratt, J. R., 1992. The Atmospheric Boundary Layer. Cambridge University Press, 316 pp.

Grimmond, C. S. B., Oke, T. R., 1999. Aerodynamic properties of urban areas derived from analysis of surface form. Journal of Applied Meteorology 38, 1262–1292.

Grimmond, C. S. B., Oke, T. R., 2002. Turbulent heat fluxes in urban areas: observations and a local-scale urban meteorological parameterization scheme (LUMPS). Journal of Applied Meteorology 41, 792—810.

Hanna, S. R., Britter, R. E., 2000. Wind flow and vapor cloud dispersion at industrial and urban sites. American Institute of Chemical Engineers/Center for Chemical Process Safety, New York, NY, 208 pp.

Hanna, S. R., Baja, E., 2009. A simple urban dispersion model tested with tracer data from Oklahoma City and Manhattan. Atmospheric Environment 43, 778-786.

825 Hanna, S. R., White, J., Trolier,J., Vernot, R., Brown, M., Kaplan, H., Alexander, Y., Moussafir, J., Wang, Y., Hannan, J., Fry, R., Kiley, C., Hendrick, E., 2009. Four diagnostic urban wind flow and dispersion models tested with Joint Urban 2003 field data. Proceedings, 30th NATO/SPS International Technical Meeting on Air Pollution Modelling and its Application, San Francisco, CA.

830 Hendricks, E., Diehl, S., Burrows, D., Keith, R., 2007. Evaluation of a fast-running urban dispersion modeling system using the Joint Urban 2003 Field Data. Journal of Applied Meteorology and Climatology 46, 2165-2179.

Jolliffe, I. T., Stephenson, D. B., 2003. Forecast Verification: A Practitioner's Guide in Atmospheric Science. Wiley and Sons, West Sussex, England, 240 pp.

835 Lenschow, D. H., Sheng Li, X., Juan Zhu, C., Stankov, B. B., 1988. The stably stratified boundary layer over the Great Plains. Boundary-Layer Meteorology 42, 95-121.

Leone Jr., J. M., Nasstrom, J. S., Maddix, D. 1997. A first look at the new ARAC dispersion model. Preprint, American Nuclear Society's Sixth Topical Meeting on Emergency Preparedness and Response, American Nuclear Society, Inc., La Grange

840 Park, IL.

Leone Jr., J. M., Nasstrom, J. S., Maddix, D. M., Larson, D. J., Sugiyama G., Ermak, D. L., 2005. Lagrangian Operational Dispersion Integrator (LODI) User's Guide. Report UCRL-AM-212798, Lawrence Livermore National Laboratory, Livermore, CA.

845 Macdonald, R. W., Griffiths, R. F., Cheah, S. C., 1997. Field experiments of dispersion through regular arrays of cubic structures. Atmospheric Environment 31, 783--795.

MacDonald, R. W., Griffiths, R. F., Hall, D. J., 1998a. An improved method for estimation of surface roughness of obstacle arrays. Atmospheric Environment 32, 1857–1864.

MacDonald, R. W., R.F. Griffiths, R. F., Hall, D. J., 1998b. A comparison of results from scaled field and wind tunnel modelling of dispersion in arrays of obstacles. Atmospheric Environment 32, 3845–3862.

MacDonald, R. W., 2000. Modelling the mean velocity profile in the urban canopy layer. Boundary-Layer Meteorology 97, 25–45.

McElroy, J. L., Pooler, F., 1968. The St. Louis Dispersion Study – Vol. II – Analysis. National Air Pollution Control Admin. Pub. No. AP-53. US DHEW Arlington, VA, 50 pp.

Nasstrom, J. S., Sugiyama, G., Leone Jr., J. M. Ermak, D. L., 2000. A real-time atmospheric dispersion modeling system. Preprint, Eleventh Joint Conference on the Applications of Air Pollution Meteorology. American Meteorological Society, Boston, MA, 84–89.

Nasstrom, J. S., Sugiyama., G., Baskett, R. L., Larsen, S. C., Bradley, M. M.., 2007. The National Atmospheric Release Advisory Center modelling and decision-support system for radiological and nuclear emergency preparedness and response. International Journal of Emergency Management 4, 524-550.

Nieuwstadt, F. T. M., 1985. A model for stationary, stable boundary layer. Turbulence and diffusion in stable environments. J. C. R. Hunt (ed.), Clarendon Press, Oxford, 149-179.

Oke, T. R., 1988: The urban energy balance. Progress in Physical Geography 12, 471–508.

Perry, S. G., 1992. A dispersion model for sources in complex topography. Part I: Technical formulations. Journal of Applied Meteorology 31, 633-645.

Piringer, M., Joffre, S. (Eds.), 2005. The urban surface energy budget and mixing height in European cities: data, models and challenges for urban meteorology and air quality. Final report of Working Group 2 of COST-715 Action. ISBN:954-9526-29-1, 239pp. Demetra Ltd. Publishers. Printed in Bulgaria.

Raupach, M. R., Thom, A. S., 1981. Turbulence in and above plant canopies. Annual Review of Fluid Mechanics 13, 97–129.

Raupach, M. R., Finnigan, J. J., Brunet, Y., 1996. Coherent eddies and turbulence in vegetation canopies: the mixing layer analogy. Boundary-Layer Meteorology 78, 351–382.

Rodean, H., 1996. Stochastic Lagrangian models of turbulence diffusion. American Meteorological Society, Boston, MA.Simpson, M., Raman, S., Lundquist, J. K., Leach, M., 2007. A study of the variation of urban mixed layer heights. Atmospheric Environment 41, 6923-6930.

Sugiyama, G., Chan, S.T., 1998. A new meteorological data assimilation model for real-time emergency response. Preprint, Tenth Joint Conference on the Applications of Air Pollution Meteorology, American Meteorological Society, Boston, MA, 285–289.

Taylor, G. I., 1921. Diffusion by continuous movements. Proceedings of the London Mathematical Society s2-20, 196–212.

Taylor, K. E., 2001. Summarizing multiple aspects of model performance in a single diagram. Journal of Geophysical Research 106, 7183-7192.

van Ulden, A. P., Holtslag, A. A. M., 1985. Estimation of atmospheric boundary layer parameters for diffusion applications. Journal of Climate Applied Meteorology 24, 1196–1207.

Warner, S., Platt, N., Heagy, J., 2004. User-oriented two-dimensional measure of effectiveness for the evaluation of transport and dispersion models. Journal of Applied Meteorology 43, 58-73.

Warner, S., Platt, N., Heagy, J., Urban, J., 2008. Comparisons of transport and dispersion model predictions of the Joint Urban 2003 field experiment. Journal of Applied Meteorology and Climatology 47, 1910-1928.

Weil, J. C., 1996. A new dispersion model for stack sources in building wakes. Preprints 9th Joint Conference on Applications of Air Pollution Meteorology with the AWMA, American Meteorological Society, Boston, 333–337.

Weil, J.C., Massman, W. J., 1996. Lagrangian stochastic modeling of scalar transport within and above plant canopies. Proceedings, 22nd Conference on Agricultural and Forest Meteorology, American Meteorological Society, Boston, J53–J57.

Figure Captions

910

Fig. 1 Schematic representation of the urban convective boundary layer, where z_i is the boundary layer height, and h is the grid-cell averaged building height.

Fig. 2 Vertical profiles of the horizontal turbulence velocity variances (left panel) and wind speed (right panel) for the second release of the fourth intensive operating
915 period of the Joint Urban 2003 field campaign (16:30 UTC / 11:30 local time, 9 July 2003). Data from the crane in black, from the urban run (URB) in blue, and from the rural run (RUR) in red.

Fig. 3 Plan view of Oklahoma City. The tracer sensor locations are depicted by the red circles, the green triangle represents the crane location, while the blue circles are
920 the release locations (Botanic gardens to the West and Westin Hotel to the East).

Fig. 4 Locations of the five surface stations and upwind profiles used in the experiments. The surface stations are Chickasha (KCHK), Wiley Post Airport (KPWA), Will Rogers World Airport (KOKC), Guthrie-Edmond Regional Airport (KGOK), and Tinker Air Force Base (KTIK), reporting wind speed and direction, temperature
925 and dew point, cloud cover fraction and station pressure. Westheimer Airport (KOUN) reported vertical profiles of wind speed and direction.

Fig. 5 The 30-min average concentration 10^{-8} g m^{-3} isosurface of the rural prediction (RUR), left panel, and the same isosurface from the urban run (URB), right panel, for the second release of IOP3 (18:30 UTC / 13:30 local time, 7 July 2003).
930 Model runs with 250 m grid increments. The wind is blowing in the figure plane, with the source located upwind of the concentration isosurface.

Fig. 6 As in Fig. 5, but with two 30-min average concentration isosurfaces (10^{-8} g m^{-3} in red and 10^{-7} g m^{-3} in blue). The wind is coming out of the figure plane.

Fig. 7 Plan view of the predicted concentration (contours, g m^{-3}) and the sensor measurements (circles, g m^{-3}) during the first release of IOP3 (16:30 UTC / 11:30 local time, 7 July 2003). The panel on the left shows the rural run (RUR), while the panel on the right is the urban run (URB).

Fig. 8 As in Fig. 7, at 17:00 UTC / 12:00 local time, 7 July 2003.

Fig. 9 Taylor diagram for the 125 m runs showing statistics computed with data from the three intensive operating periods. The azimuthal position gives the correlation between observation and predictions (paired in space and time), while the radial distance from the origin is proportional to the normalized standard deviation (standard deviation of predictions over standard deviation of observations). The arrow tails represent the statistics of the rural runs (RUR), while the arrow heads represent the urban runs (URB). The red square on this diagram represents the observations. The distance on the diagram between the point representing the forecast and the red square representing the observations is the centered root mean square error. The above metrics have been computed by grouping the concentration sensors as all the sensors together (black arrow), the sensors in the urban core (green arrow), and the sensors at the three downwind (1 km, 2 km, and 4 km) arcs (light blue, magenta, and blue arrows, respectively).

Fig. 10 Taylor diagram for the 250 m runs (similar to Fig. 9).

Fig. 11 Taylor diagram for the 500 m runs (similar to Fig. 9).

Fig. 12 Taylor diagram for the 1000 m runs (similar to Fig. 9).

Fig. 13 Fractional Bias (FB) values computed with data from the three intensive operating periods, for the five groups of sensors (all, urban core, first, second and third arc), and for each of the four grid increments (1000, 500, 250, and 125 m). For each of grid increment, the left bar represents the FB of the rural run (RUR), while the right bar is for the urban run (URB).

Fig. 14 Measure of effectiveness (MOE) computed with data from the three intensive operating periods, for the five groups of sensors (all, urban core, first, second and third arc), and for the runs with 250 m grid increments. The rural runs (RUR) values are shown with open squares, while the solid squares correspond to MOE values associated with the urban runs (URB). The perfect MOE is (1, 1), and corresponds to complete overlap of the predicted and observed plumes. MOE values on the 1:1 line indicate that the observed and predicted plumes have the same area, but their locations may be different. An increasing value of the abscissa corresponds to a decreasing number of false negative alarms, whereas an increasing value of the ordinate indicates a decreasing number of false positives.

Table 1. The 10-min vector-average wind speed and wind direction values from the z = 42.5 m level at the crane site, averaged over the duration of the continuous release measurement (Flaherty et al., 2007a)

IOP	Date	Release time (UTC)	Release rate ($g\ s^{-1}$)	Release location	Averaged wind speed ($m\ s^{-1}$)	Averaged wind direction (◦)
2	2 July 2003	1600-1630 1800-1830 2000-2030	5.0 5.0 5.0	Westin Hotel	3.9	204
3	7 July 2003	1600-1630 1800-1830 2000-2030	5.0 3.0 3.0	Botanic gardens	5.6	188
4	9 July 2003	1600-1630 1800-1830 2000-2030	3.1 3.0 3.0	Botanic gardens	6.0	194

975

Table 2. Fractional Bias (FB), correlation (Corr.), and normalized standard deviation (NSD) calculated for the five sensor groups, by representing the source either as a point source or as a Gaussian source.

Metric	Source Geometry	All Sensors	Urban Core	First Arc (1 km)	Second Arc (2 km)	Third Arc (4 km)
FB	**Point**	0.62	0.63	0.33	0.39	0.13
	Gaussian	0.40	0.40	0.40	0.39	0.13
Corr.	**Point**	0.38	0.36	0.70	0.71	0.52
	Gaussian	0.47	0.45	0.71	0.66	0.50
NSD	**Point**	1.23	1.20	0.98	1.26	1.09
	Gaussian	0.79	0.77	1.17	1.38	1.14

980

Table 3. Comparison of the urban parameterization presented in this paper (DM09) with different modeling systems tested with the Joint Urban data set (Chan and Leach, 2007 (C07); Hendricks et al., 2007 (H07); Warner et al., 2008 (W08)). The metrics include Fractional Bias (FB), correlation (Corr.), factor of 2 (FAC2), and the measure of effectiveness (MOE), and are computed with the sensors in the central business district of Oklahoma City, Oklahoma. For W08 the reported values are ranges corresponding to a series of runs.

Reference	**Model**	**Period**	**FB**	**Corr**	**FAC2**	**MOE** $(\frac{A_{o\ v}}{A_{o\ b}}, \frac{A_{o\ v}}{A_{p\ r}})$
C07 (Section 4.a)	FEM3MP	IOP3	-0.56	N/A	< 0.42*	N/A
H07 (Table 4)	RUSTIC/MESO	Daytime	0.16	0.15	0.44	N/A
W08 (Fig. 8, Table 5)	Urban HPAC	Daytime	[-0.90, -0.55]	N/A	[0.44, 0.56]**	(0.59, 0.42)
DM09 (Table 2)	ADAPT/LODI (250 m)	IOP2-3-4	0.40	0.45	0.24/ 0.39***	(0.62, 0.34)

*The upper limit for FAC2 of C07 is the factor of 5 value.
**FAC2 of W08 are computed with all the sensors.
***FAC2 of DM09 with CBD sensors/all sensors.

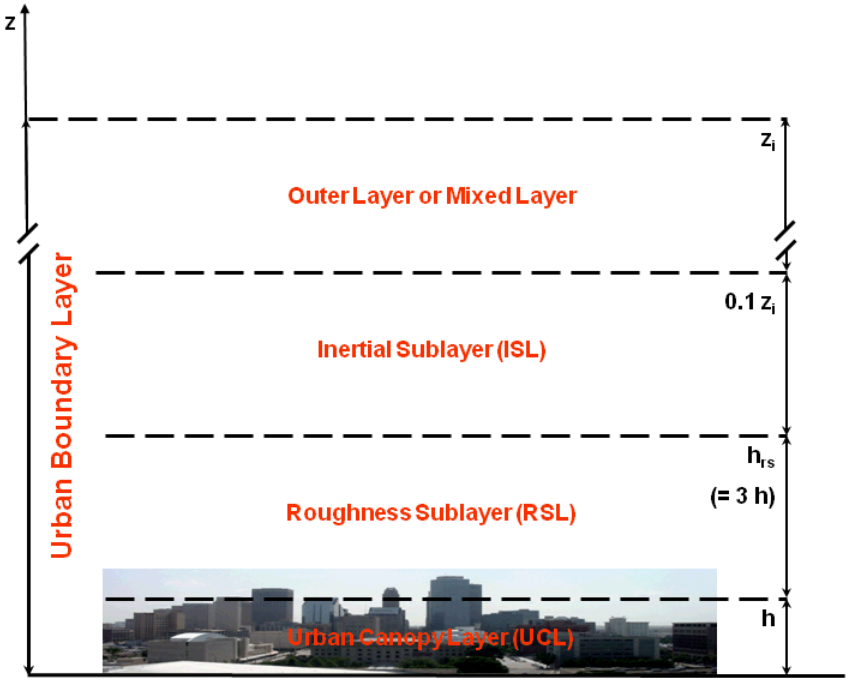

Fig. 1 Schematic representation of the urban convective boundary layer, where z_i is the boundary layer height, and h is the grid-cell averaged building height.

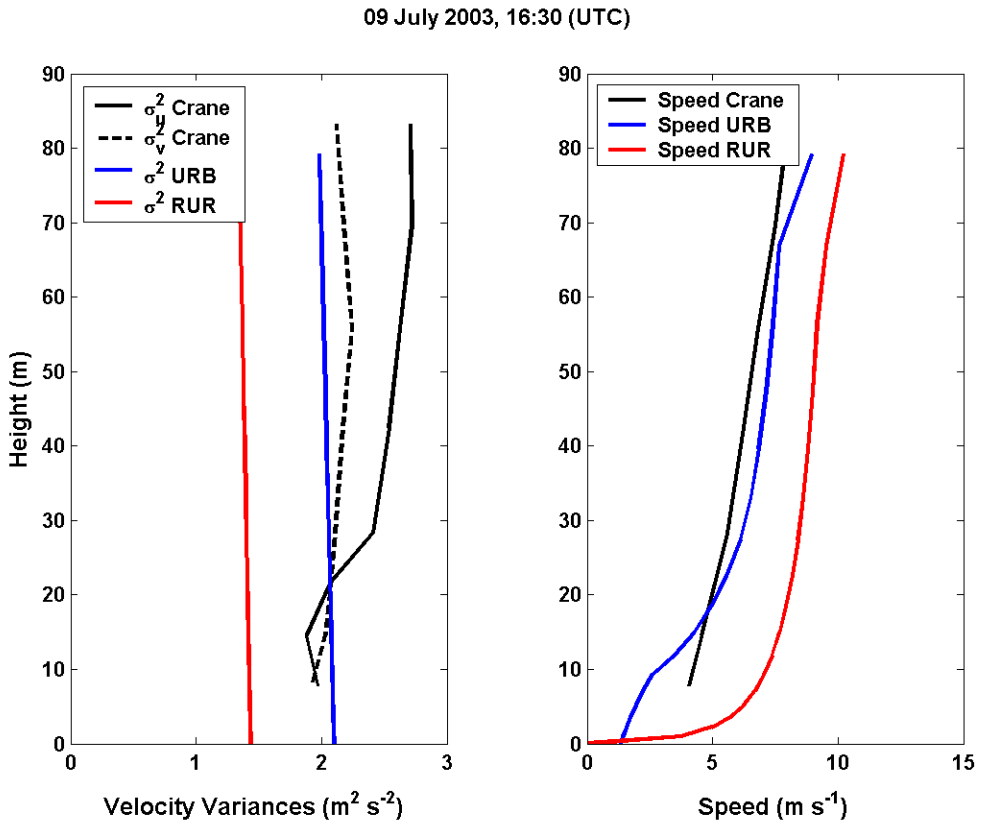

Fig. 2 Vertical profiles of the horizontal turbulence velocity variances (left panel) and wind speed (right panel) for the second release of the fourth intensive operating period of the Joint Urban 2003 field campaign (16:30 UTC / 11:30 local time, 9 July 2003). Data from the crane in black, from the urban run (URB) in blue, and from the rural run (RUR) in red.

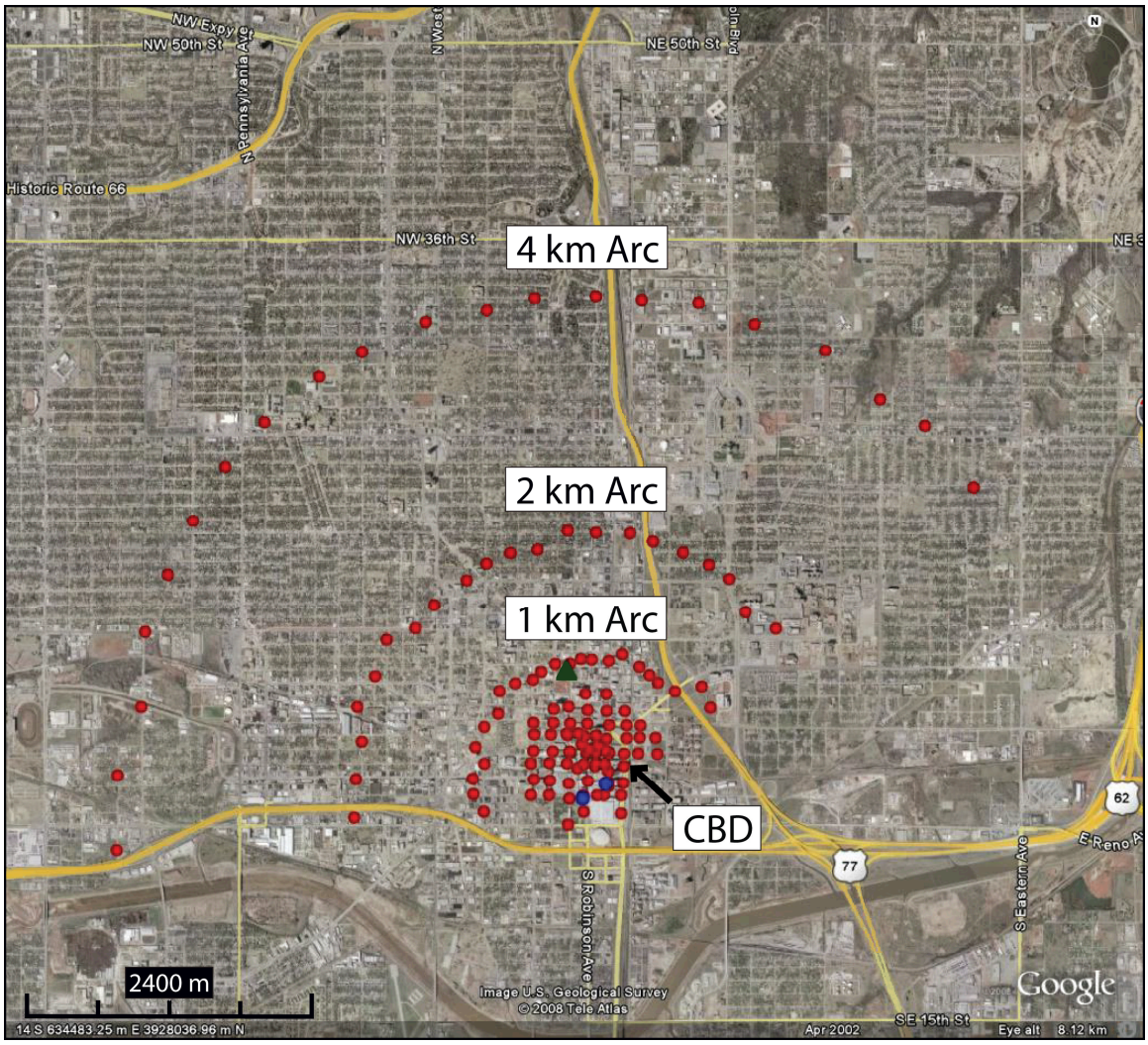

1005 **Fig. 3** Plan view of Oklahoma City. The tracer sensor locations are depicted by the red circles, the green triangle represents the crane location, while the blue circles are the release locations (Botanic gardens to the West and Westin Hotel to the East).

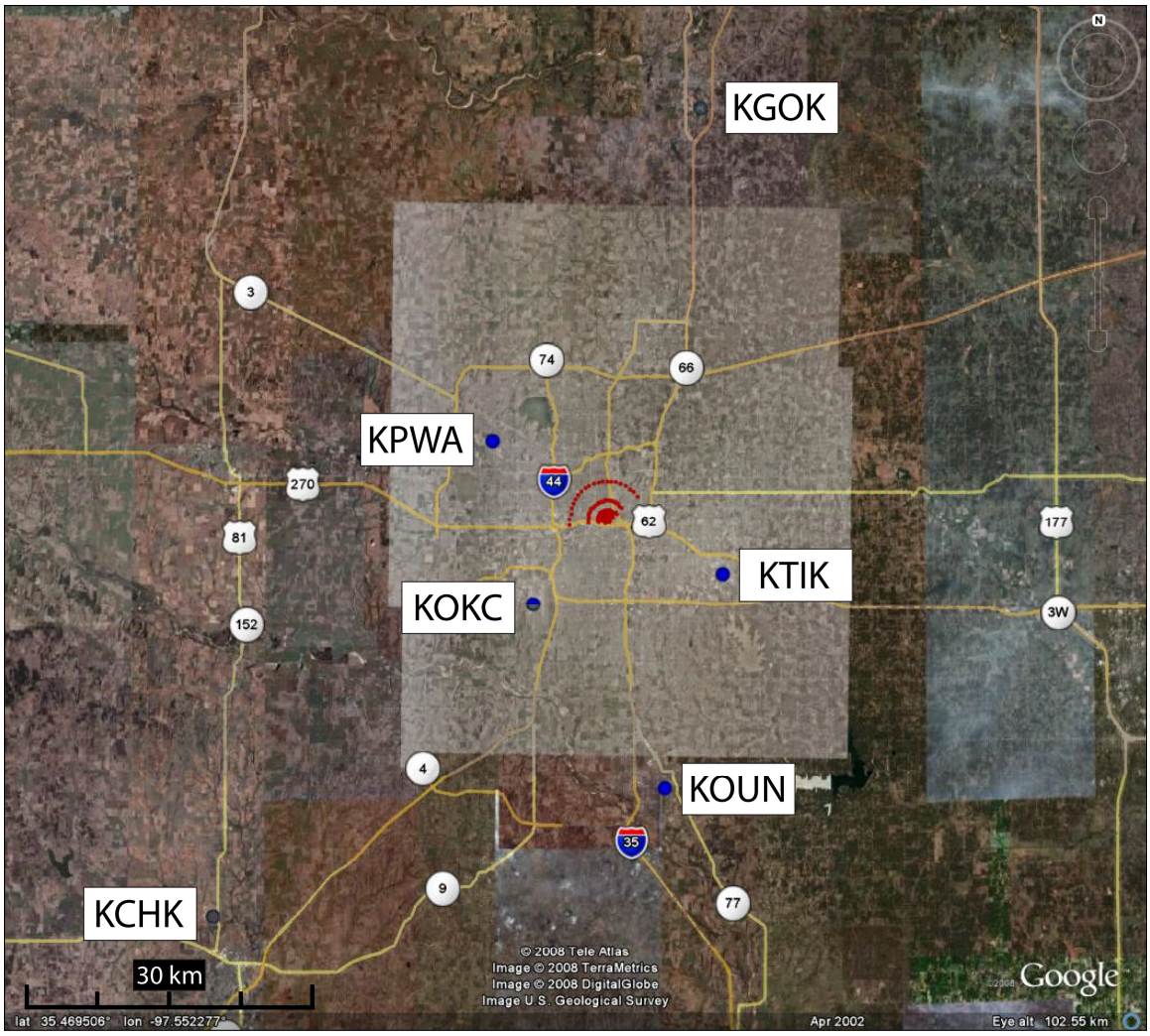

1010 **Fig. 4** Locations of the five surface stations and upwind profiles used in the experiments. The surface stations are Chickasha (KCHK), Wiley Post Airport (KPWA), Will Rogers World Airport (KOKC), Guthrie-Edmond Regional Airport (KGOK), and Tinker Air Force Base (KTIK), reporting wind speed and direction, temperature and dew point, cloud cover fraction and station pressure. Westheimer Airport (KOUN) reported vertical

1015 profiles of wind speed and direction.

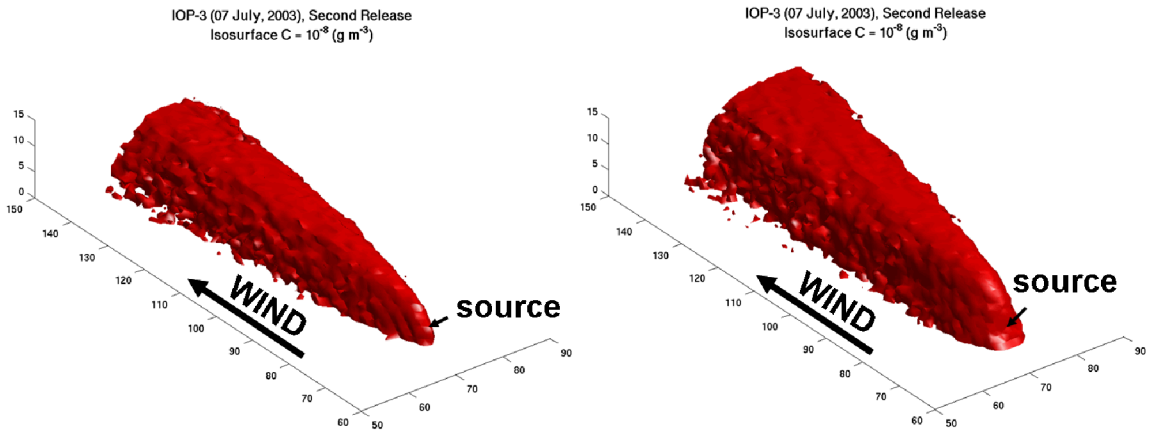

Fig. 5 The 30-min average concentration 10^{-8} g m^{-3} isosurface of the rural prediction (RUR), left panel, and the same isosurface from the urban run (URB), right panel, for the second release of IOP3 (18:30 UTC / 13:30 local time, 7 July 2003). Model runs with 250 m grid increments. The wind is blowing in the figure plane, with the source located upwind of the concentration isosurface.

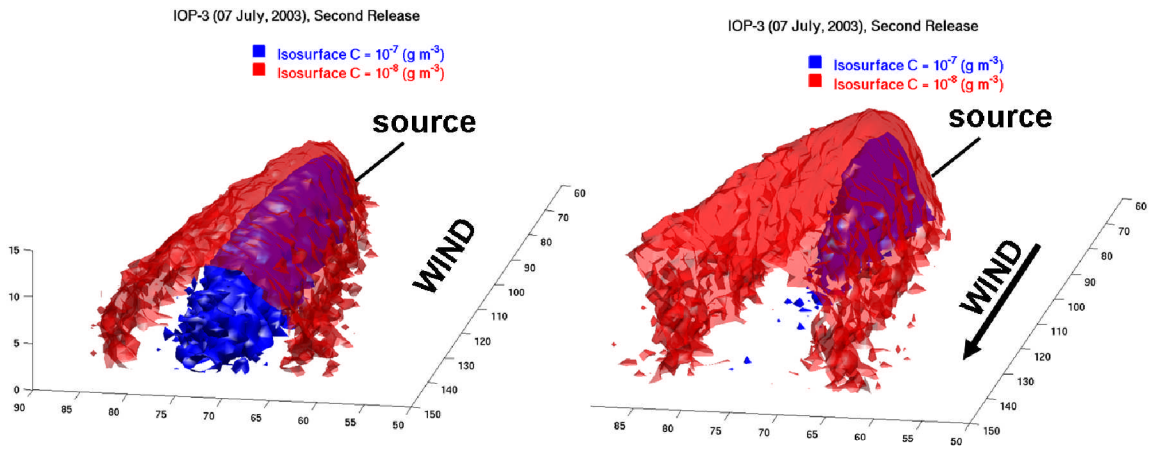

1025 **Fig. 6** As in Fig. 5, but with two 30-min average concentration isosurfaces (10^{-8} g m^{-3} in red and 10^{-7} g m^{-3} in blue). The wind is coming out of the figure plane.

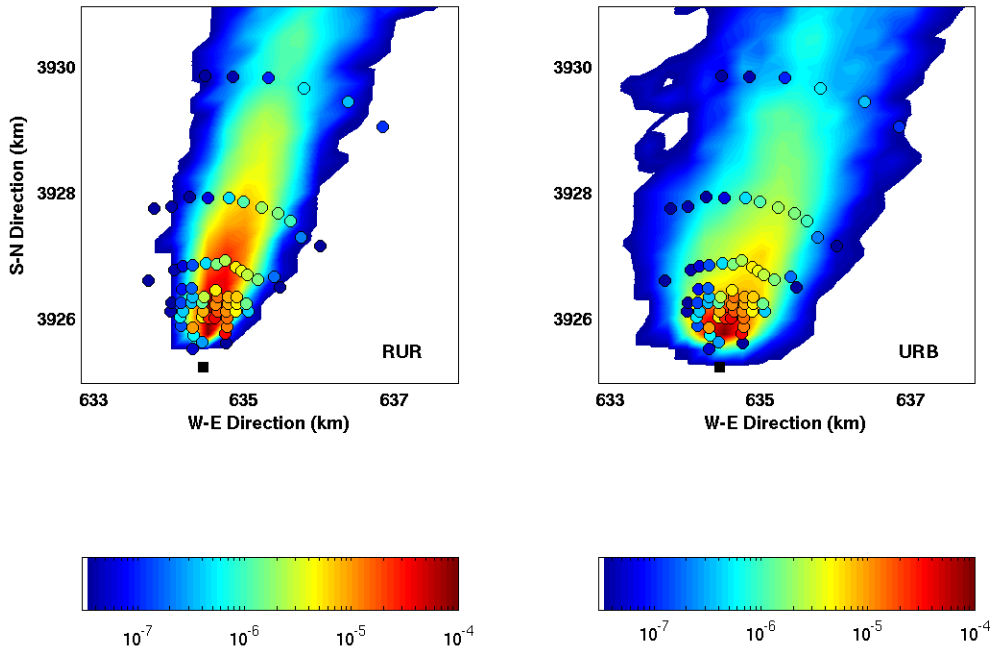

Fig. 7 Plan view of the predicted concentration (contours, g m^{-3}) and the sensor measurements (circles, g m^{-3}) during the first release of IOP3 (16:30 UTC / 11:30 local time, 7 July 2003). The panel on the left shows the rural run (RUR), while the panel on the right is the urban run (URB).

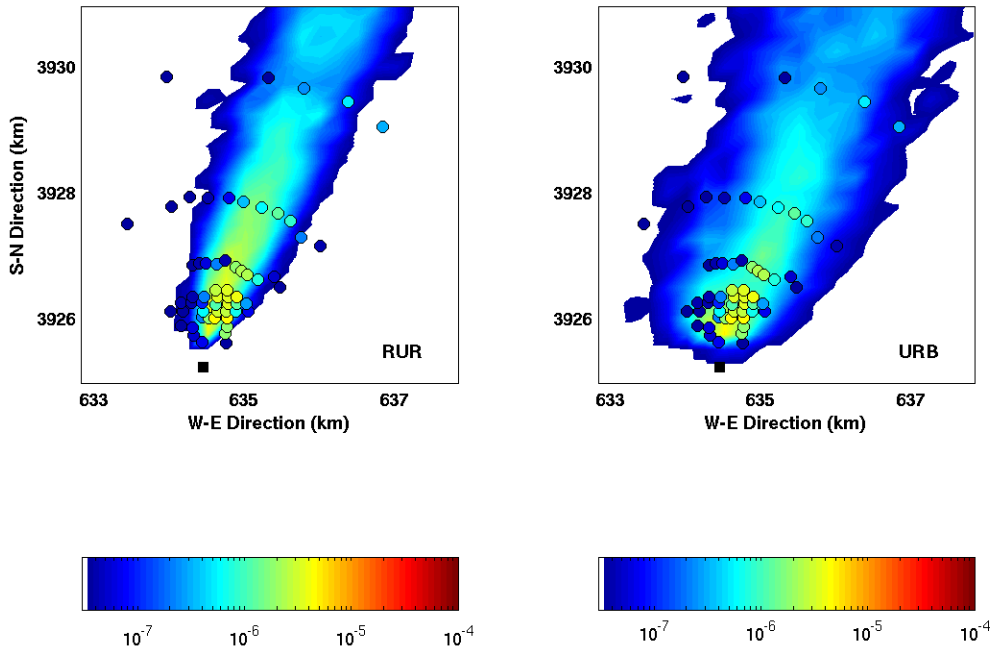

1035 **Fig. 8** As in Fig. 7, at 17:00 UTC / 12:00 local time, 7 July 2003.

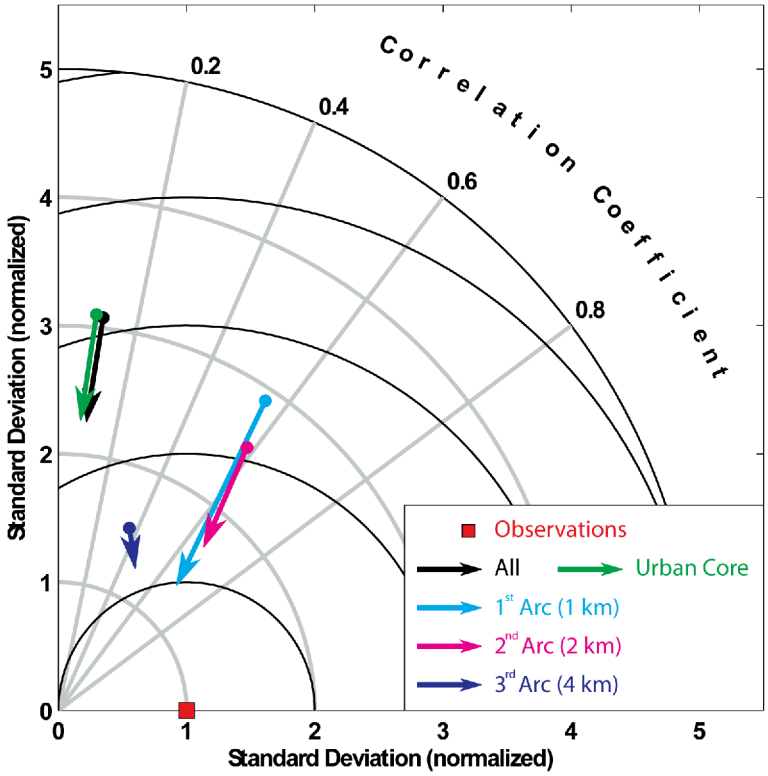

Fig. 9 Taylor diagram for the 125 m runs showing statistics computed with data from the three intensive operating periods. The azimuthal position gives the correlation between observation and predictions (paired in space and time), while the radial distance from the origin is proportional to the normalized standard deviation (standard deviation of predictions over standard deviation of observations). The arrow tails represent the statistics of the rural runs (RUR), while the arrow heads represent the urban runs (URB). The red square on this diagram represents the observations. The distance on the diagram between the point representing the forecast and the red square representing the observations is the centered root mean square error. The above metrics have been computed by grouping the concentration sensors as all the sensors together (black arrow),

the sensors in the urban core (green arrow), and the sensors at the three downwind (1 km, 2 km, and 4 km) arcs (light blue, magenta, and blue arrows, respectively).

1050

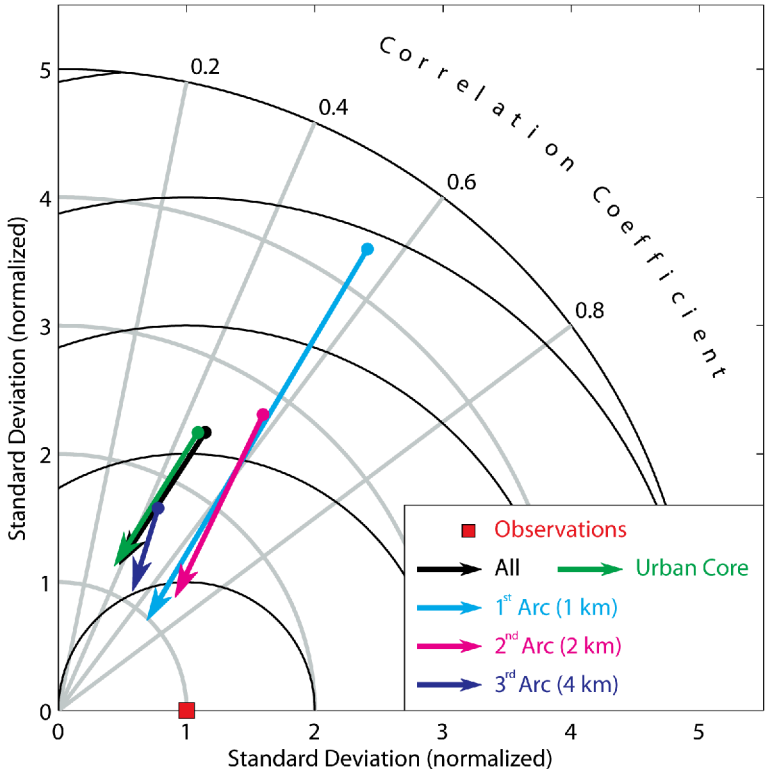

Fig. 10 Taylor diagram for the 250 m runs (similar to Fig. 9).

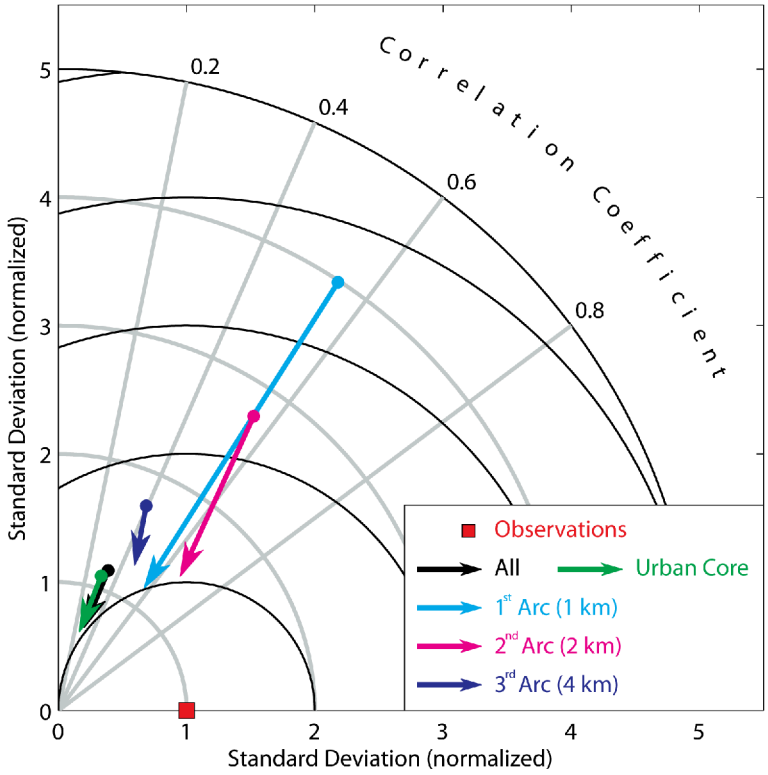

1055 **Fig. 11** Taylor diagram for the 500 m runs (similar to Fig. 9).

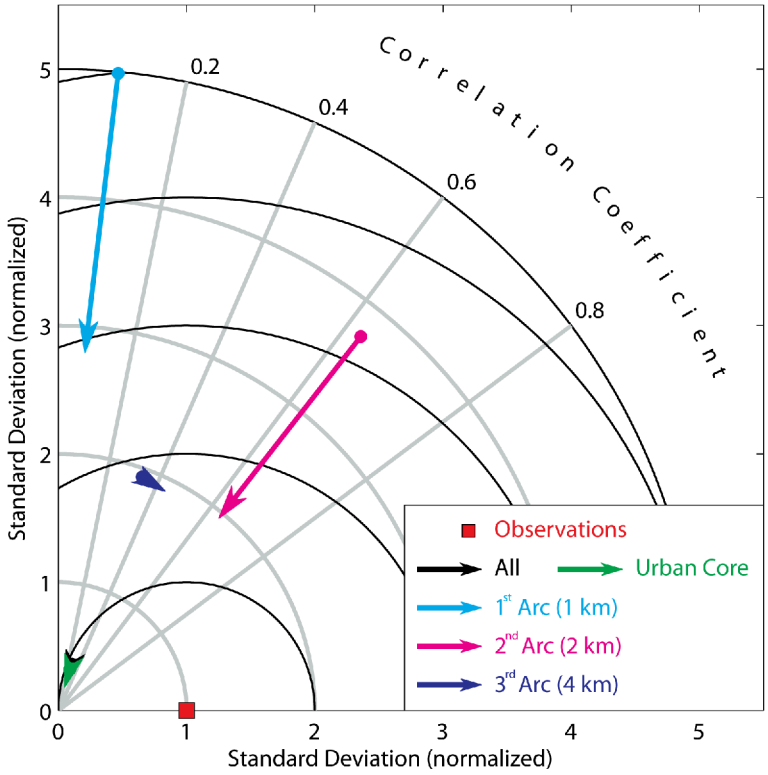

Fig. 12 Taylor diagram for the 1000 m runs (similar to Fig. 9).

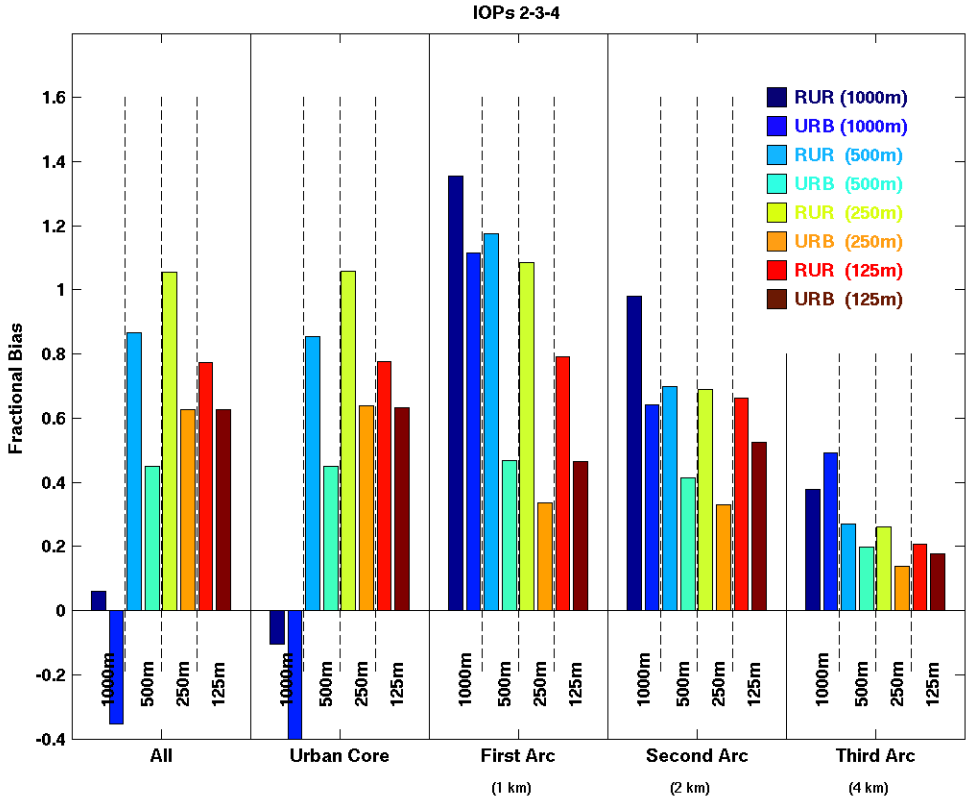

1060

Fig. 13 Fractional Bias (FB) values computed with data from the three intensive operating periods, for the five groups of sensors (all, urban core, first, second and third arc), and for each of the four grid increments (1000, 500, 250, and 125 m). For each of grid increment, the left bar represents the FB of the rural run (RUR), while the right bar is for

1065 the urban run (URB).

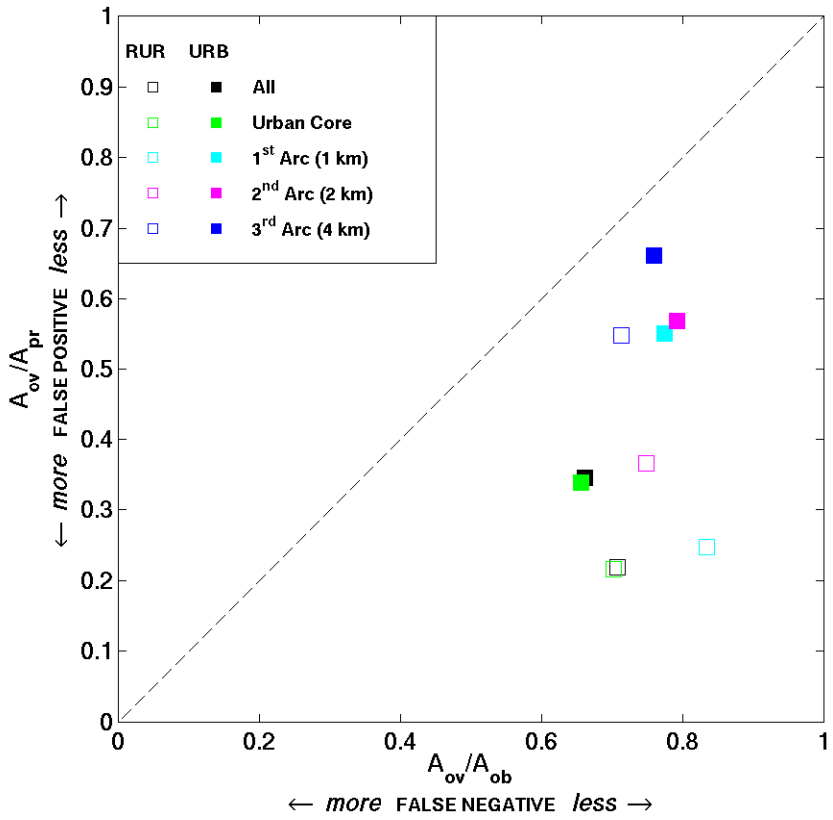

Fig. 14 Measure of effectiveness (MOE) computed with data from the three intensive operating periods, for the five groups of sensors (all, urban core, first, second and third arc), and for the runs with 250 m grid increments. The rural runs (RUR) values are shown with open squares, while the solid squares correspond to MOE values associated with the urban runs (URB). The perfect MOE is (1, 1), and corresponds to complete overlap of the predicted and observed plumes. MOE values on the 1:1 line indicate that the observed and predicted plumes have the same area, but their locations may be different. An increasing value of the abscissa corresponds to a decreasing number of false negative alarms, whereas an increasing value of the ordinate indicates a decreasing number of false positives.